Laser and Particle Beams (2013), *31*, 233–238.

doi:10.1017/S0263034613000220

Ultra-intense attosecond pulses emitted from laser wakefields in non-uniform plasmas

Y. LIU,[1] F.Y. LI,[1] M. ZENG,[1] M. CHEN,[1,2] AND Z.M. SHENG[1,2]

[1]Key Laboratory for Laser Plasmas (Ministry of Education) and Department of Physics and Astronomy, Shanghai Jiao Tong University, Shanghai, China

[2]Department of Mathematics, Institute of Natural Sciences, and MOE-LSC, Shanghai Jiao Tong University, Shanghai, China

(Received 15 February 2013; Accepted 17 March 2013)

Abstract

A scheme of generating ultra-intense attosecond pulses in ultra-relativistic laser interaction with under-dense plasmas is proposed. The attosecond pulse emission is caused by an oscillating transverse current sheet formed by an electron density spike composed of trapped electrons in the laser wakefield and the residual transverse momentum of electrons left behind the laser pulse when its front is strongly modulated. As soon as the attosecond pulse emerges, it tends to feed back to further enhance the transverse electron momentum and the transverse current. Consequently, the attosecond pulse is enhanced and developed into a few cycles later until the density spike is depleted out due to the pump laser depletion. To control the formation of the transverse current sheet, a non-uniform plasma slab with an up-ramp density profile in front of a uniform region is adopted, which enables one to obtain attosecond pulses with higher amplitudes than that in a uniform plasma slab.

Keywords: Attosecond pulses; Laser wakefields; Non-uniform plasmas; Residual transverse momentum

1. INTRODUCTION

The generation of attosecond pulses (APs) opens the possibility to probe and even manipulate ultra-fast electron dynamics occurring in atomic structures (Von der Linde *et al.*, 2001; Corkum & Krausz, 2007; Mourou *et al.*, 2007; Midorikawa, 2011). Currently, the well-known schemes to produce APs include high harmonics generation (HHG) from laser-atom interaction at moderate laser intensity (Salieres *et al.*, 1995; Hergott *et al.*, 2002; Takahashi *et al.*, 2004; Nabekawa *et al.*, 2009) or HHG from laser-solid interaction at relativistic laser intensity (Naumova *et al.*, 2004; Quere *et al.*, 2006; Tsakiris *et al.*, 2006; Zheng *et al.*, 2006; Baeva *et al.*, 2007; Dromey *et al.*, 2009). Other schemes include the Thomson scattering from current sheets (Meyer-ter-Vehn & Wu, 2009; Wu *et al.*, 2010) and flying mirrors (Roso *et al.*, 2000; Bulanov *et al.*, 2003; Kando *et al.*, 2007), which are produced in the relativistic laser interaction with thin-solid targets and from laser wakefields driven in under-dense plasma, respectively.

Recently, we proposed that APs may be produced directly from such laser wakefields (Liu *et al.*, 2012). The generation process of APs can be described as follows. When an ultra-relativistic laser pulse propagates through a uniform plasma slab, a sharp electron density spike in the wakefields is generated behind the driving laser pulse. In homogeneous plasma, the relationship between electron density and the phase velocity of a wake can be described by $n = n_0/(1 - \beta/\beta_{ph}$, where n_0 is the initial electron density, β and β_{ph} are the electron fluid velocity and the phase velocity of the wakefield normalized by the vacuum speed of light c, respectively. From such a relation, a density spike with the maximum density n_{max} will be found near the maximum electron fluid velocity β_m (normalized by c), and its width is given by $d = (2(\beta_{ph} - \beta_m)^2/[\beta_m\ (1 - \beta_m^2)^{3/2}])^{1/2}$ in the cold plasma limit (Bulanov *et al.*, 1998). Next, as the intense laser pulse continues to propagate in plasmas, its front becomes steepened gradually due to the relativistic self-modulation and due to the plasma density modulation at the front caused by the longitudinal ponderomotive force of the laser pulse (Decker *et al.*, 1996). As a result, the carrier phase of the laser pulse evolves with time in such a way that the transverse momentum of electrons located behind the laser pulse is nonzero, i.e., $p_z\ (x_0\ , t) = a(x_0, t) = -\int_{-\infty}^{t} cE_z(x_0, t')dt'$, where $a(x_0, t)$ is the vector potential at a given position x_0 and $E_z(x_0, t)$ is the transverse electric field at x_0 along the z-direction, which is the laser polarization direction. This evolving transverse momentum left behind the

Address correspondence and reprint requests to: Zheng-Ming Sheng, Department of Physics, Shanghai JiaoTong University, 800 Dongchuan Road, Minhang, Shanghai 200240, China. E-mail: zmsheng@sjtu.edu.cn

laser pulse is called the residual transverse momentum since it only develops quickly after the laser has propagated over a certain distance. Finally, the density peak trapped in the laser wakefield and the transverse momentum of electrons behind the laser pulse form a net transverse current sheet env_z, which comoves with the laser pulse and radiates an electromagnetic pulse at the frequency characterized by the c/d with d being the thickness of the density spike mentioned above. Our previous studies (Liu *et al.*, 2012) suggest that the emitted pulse is typically in the extreme ultraviolet range with the pulse duration in a few hundred attoseconds in one-dimensional simulations and few femtoseconds in multi-dimensional simulations. In the latter case, the emitted pulse energy can be as large as a few mJ with the pump laser around 20 J.

In the present work, we show that the AP emission produced in this way can be further intensified when an up-ramp density profile is used in front of a uniform plasma slab. This is associated with the controlled formation of the oscillating current sheet in the laser wakefield driven behind the laser pulse, which enables the current sheet produced with a higher peak value and narrower width. The paper is arranged as follows. In Section 2, the mechanism of the AP emission is clarified and the effects of up-ramp density profile as well as the laser polarization are discussed. In Section 3, two-dimensional effects are introduced. The paper concludes a summary in Section 4.

2. GENERATION OF ATTOSECOND PULSES IN NONUNIFORM PLASMAS

To simplify the problem, we consider the laser pulse propagation and laser wakefield excitation in a non-uniform plasma slab with mobile ions as shown in Figure 1. The plasma density first increases linearly from zero to $n_0/n_c = 0.04$ in a length of 70μm and then keeps constant for 100 μm, where $n_c = m_e\omega_L^2/4\pi e^2$ is the critical density for a driver pulse with frequency ω_L. Such a density profile can be produced with a gas nozzle. A laser pulse is incident from the left boundary of the simulation box and propagates along the x-direction. It is linearly-polarized with the peak intensity of 1.37×10^{20} W/cm^2 (corresponding to the normalized vector potential $a_0 = 10$ at the wavelength $\lambda_L = 1$ μm), the full laser period is $\tau = 10T_L$ for a sine square pulse with T_L the oscillating period. Numerical simulations are conducted with the code KLAPS-1D (Sheng *et al.*, 2000; Chen *et al.*, 2008; Wang *et al.*, 2010). We use a simulation cell size of $\lambda_L/200$ to ensure enough resolutions both in time and space.

Figure 2a shows the snapshot of the spatial distributions of the electron density and the electric fields at $t = 150T_L$. Besides a density peak located in the front part of the laser pulse, a high density spike is found at the end of the first wake bucket. At this second density peak, an ultra-short pulse shows up. The inset displays the zoomed-in plot of this short pulse, which has a full width about 270*as*. The second electron density spike in Figure 2a behind the laser

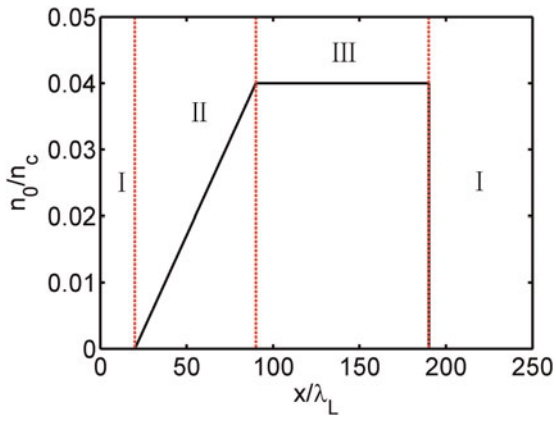

Fig. 1. (Color online) Longitudinal line-out of the initial plasma electron density profile. The laser pulse propagates from left to right.

pulse is due to wave breaking and electron trapping when the laser pulse propagates across the density transition point at time $t = 110T_L$. This kind of electron trapping realizes the synchronized injection of electrons in the first wave when the wake phase velocity suddenly drops from superluminality to well below c after the long-term process

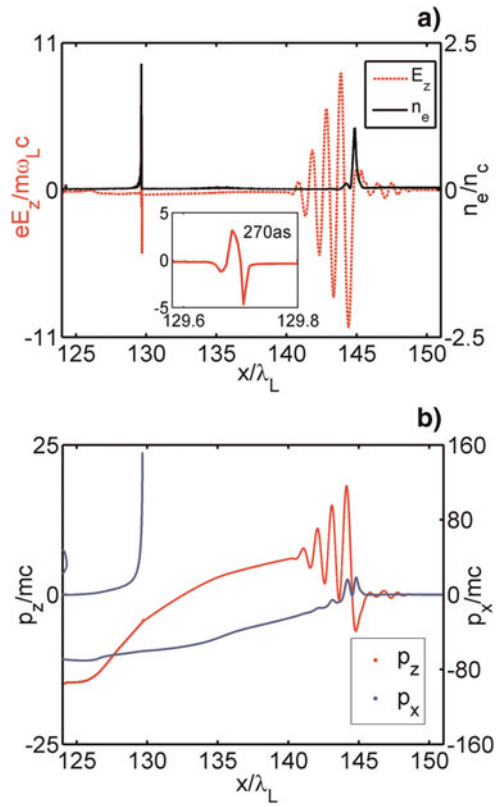

Fig. 2. (Color online) (**a**) Laser field (normalized by $m\omega_L c/e$, red dashed line) and the electron density (normalized by n_c, black solid lines) are plotted at the time $t = 100T_L$. It shows an AP with a full duration 270*as* (red solid line in the inset) is produced near the electron density spike behind the laser pulse. (**b**) Longitudinal distributions of the longitudinal (red dotted line) and transverse (blue dotted line) momenta of electrons.

https://doi.org/10.1017/S0263034613000220 Published online by Cambridge University Press

of wake-breaking suppression (Li *et al.*, 2012). Figure 2b plots the longitudinal distributions of the electron momenta. It shows that the AP emission locates at almost the same position as the density spike, where the transverse residual momenta of the electrons are nonzero.

Figure 3 displays the temporal evolution of the density peak value, the transverse electron momentum and the transverse current density along the laser polarization direction. In the simulation, we find the maximum density of the second density peak is about $7.5\underline{n}_c$ near $t = 100T_L$. At this time, the transverse momentum keeps oscillating with small amplitude. However, the transverse current density begins to oscillate violently after that. The AP is produced according to the wave equation $(\partial^2/\partial x^2 - c^{-2}\partial^2/\partial t^2)E_z = (4\pi/c^2)\partial j_{z,spike}/\partial t$, the emitted pulse is given by $E_z = 4\pi\gamma_g^2 \frac{v_g^2}{c^2}\int_{-\infty}^{\tau} j_{z,spike}(\tau')d\tau'$, where $j_{z,\mathrm{spike}}(\tau)$ with $\tau = t - v/g$ is the transverse electron current near the density peak, $\gamma_g = (1 - v_g^2/c^2)^{-1/2}$ with v_g the group velocity of the laser radiation in the ambient plasma. Once the AP appears, the residual transverse momentum is further enhanced locally at the AP position with $p_z(x_0, t) = -\int_{-\infty}^{t} cE_z(x_0, t')dt'$ and then the transverse current density becomes enhanced further subsequently in view of the violent evolution of p_z, which is shown to oscillate with time in a period about $25T_L$. Then it feeds back to the formation of the AP and the first positive loop is complete. Figure 3 shows that the transverse current density starts to develop dramatically at $t = 110T_L$ and the transverse residual momentum begins to oscillate vigorously at $t = 130T_L$ due to the emission of APs. One notes that the normalized maximum field approaches 5 at $t = 130T_L$, corresponding to the intensity of 3.4×10^{19} W/cm^2. After $t = 130T_L$, the peak density starts to decrease. This happens when the electrons forming the ultra-short density spike slip out of the accelerating phase of the wakefield. When the density peak is reduced remarkably, the transverse electron momentum and current density decrease correspondingly until the density spike disappears completely. Eventually, the density spike disappears after $t = 190T_L$ when the laser pulse propagates out of the plasma and the AP evolution comes to the end and propagates out of the plasma with three cycles as shown in Figure 4. This is consistent with the oscillation cycles of the transverse electron momentum undergoes during the period between $t = 130T_L$ and $t = 190T_L$. The pulse shape and spectrum of the AP in vacuum after passing through the plasma region are shown in Figure 4. We can see that the ultra-short pulse covers a broad spectrum range with the maximum frequency extending to $100\omega_L$.

To show the effects of using an up-ramp density profile, Figure 5 plots the AP amplitude and duration produced with different laser strengths or variable initial maximum electron density for the cases of uniform plasma and non-uniform plasma with an up-ramp density profile. These simulations reveal that the peak amplitude of the produced APs in plasma with an up-ramp is 5–10 times of that in uniform plasma, while the AP period is only a half of that in uniform plasma. This shows obviously the advantage of using an up-ramp density profile. Figures 5a and 5c indicate that the peak amplitude of the APs generally increases with the laser intensity or the maximum plasma density regardless of the density profiles. On the other hand, Figures 5b and

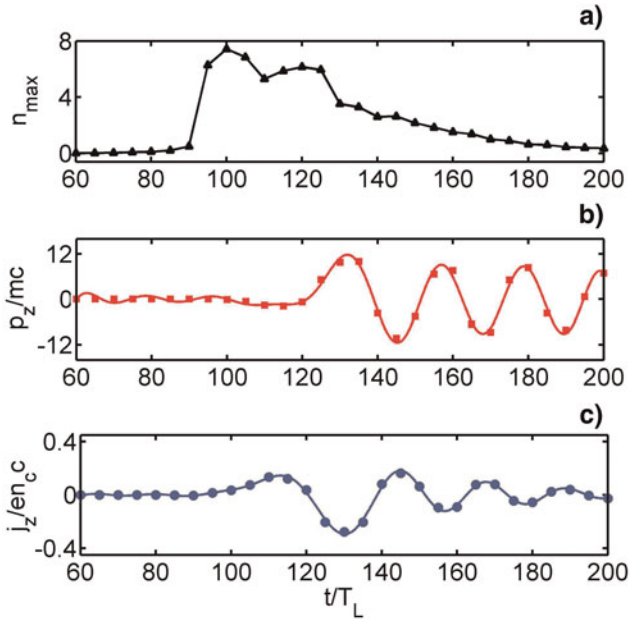

Fig. 3. (Color online) (**a**) Evolution of the maximum electron density in the density spike behind the laser pulse. (**b**) Temporal evolution of the residual transverse momentum of electrons near the density spike at 20 μ*m* away from the front of the laser pulse. (**c**) Evolution of the maximum transverse current density in the current sheet.

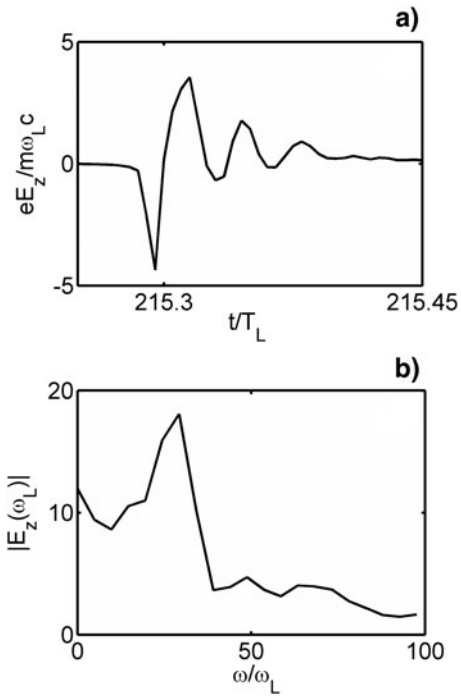

Fig. 4. Electric field of the emitted AP at the right side of the plasma slab in vacuum (**a**) and the corresponding frequency spectrum (**b**).

https://doi.org/10.1017/S0263034613000220 Published online by Cambridge University Press

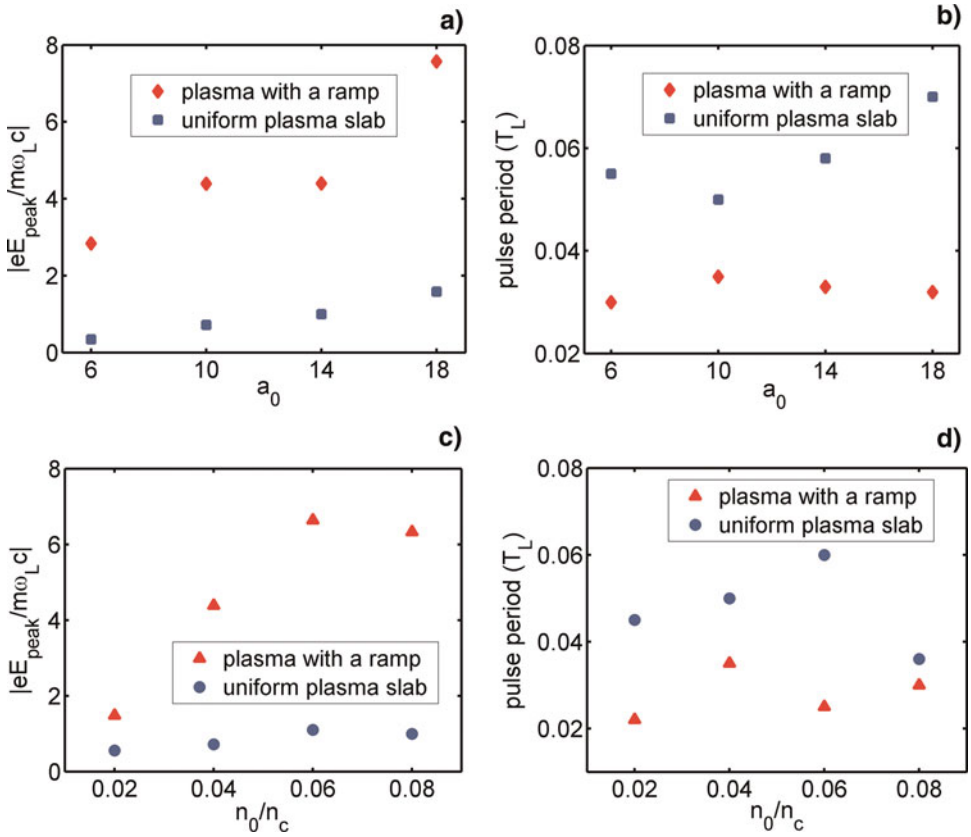

Fig. 5. (Color online) Comparison of AP generation in uniform plasma and in nonuniform plasma with an up-ramp density profile. Plots (**a**) and (**b**) show the normalized peak amplitude and duration of the AP versus the driving laser amplitude, respectively, for a fixed maximum density $n_0/n_c = 0.04$. Plots (**c**) and (**d**) show the normalized peak amplitude and duration of the AP versus the maximum plasma density, respectively, for a fixed driving laser amplitude $a_0 = 10$.

5d display that the period of APs does not change significantly with the laser and plasma parameters. In the case with the up-ramp non-uniform plasma, the AP period always keeps as short as 100*as*, suggesting that the period of the APs is not very sensitive to the laser intensity and the maximum plasma density. In non-uniform plasmas, the laser pulse evolves for much longer time before the density spike shows up and electron trapping occurs. This means the initial transverse electron momentum is larger than that for the case of uniform plasma. Therefore, combined with the large electron injection at the density transition point, the AP produced has higher amplitude and a shorter period when an up-ramp density profile is used. We also have checked the effect on the length in the up-ramp region. Generally the attosecond pulse duration and amplitude are not very sensitive to this length as long as it is larger than a few plasma wavelengths, though there are some small fluctuations in the AP amplitudes with different lengths in the up-ramp region.

Previous simulation has taken linearly-polarized laser pulses and the produced APs have the same polarization of the driving lasers. We have checked the effect with a circularly polarized (CP) laser pulse. In the simulation, we take the same conditions as before for Figure 4 except the laser pulse is circularly polarized with the reduced peak amplitude $a_L = 10/\sqrt{2}$ (note that the corresponding laser intensity is the same as before). In this case, large residual transverse momentum is found in both transverse directions. Subsequently, the produced AP is almost circularly polarized. Figure 6a presents the two electric field components, which have a $\pi/2$ phase difference and their spectra are quite similar.

3. TWO-DIMENSIONAL EFFECTS

As shown above, the AP generation in the laser wakefield is basically a one-dimensional effect. In a real situation, the laser pulses always have a finite transverse spot size. To check the effects of the finite laser spot size, we have performed two-dimensional PIC simulations with the code OSIRIS 2.0 (Fonseca *et al.*, 2002), where similar laser and plasma conditions as one-dimensional simulation have been used and a transverse Gaussian envelope with a waist size $w_r = 20\lambda$ is used. Usually a large laser spot size is preferred for AP generation (Liu *et al.*, 2012). In the simulation, a moving window is taken with the size of $50 \times 100\ \lambda_L^2$ and approximately 10^9 particles are chosen. High spatial resolution of $0.005\lambda_L$ is taken as similar to the one-dimensional case.

https://doi.org/10.1017/S0263034613000220 Published online by Cambridge University Press

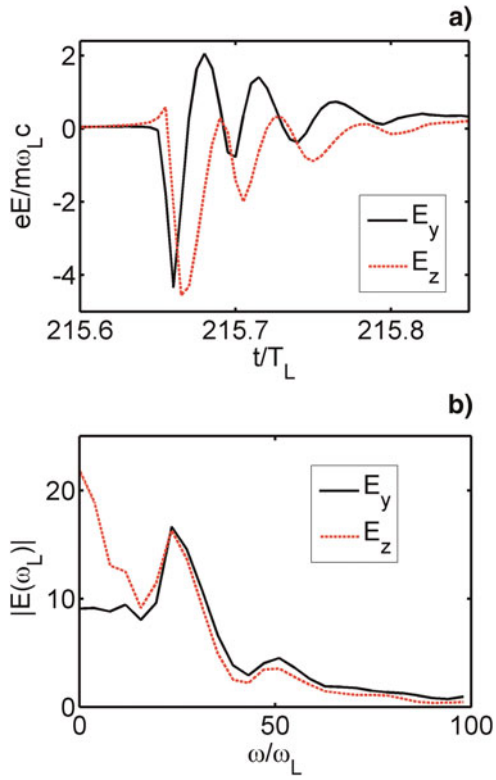

Fig. 6. (Color online) Two components of the electric fields of the emitted APs produced by a CP pulse (**a**) and the corresponding frequency spectra (**b**).

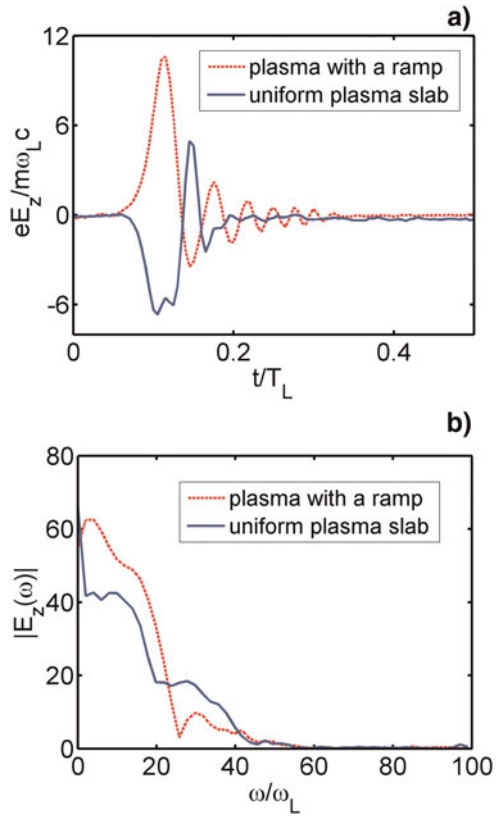

Fig. 7. (Color online) APs from two-dimesnional PIC simulations for the same laser and plasma (uniform or non-uniform) parameters as in Figure 2. (**a**) Snapshot of the electric field in the laser polarization direction. (**b**) Spectrum of the APs.

With a uniform plasma slab, it has been found before that the produced ultra-short pulse is usually as short as a few femtoseconds in two-dimensional simulation instead of a few hundred attoseconds found in one-dimensional simulation (Liu *et al.*, 2012). In the meanwhile, the frequency spectrum width is also reduced from the one-dimensional result. In the case with a non-uniform plasma slab, though generally the emitted ultra-short XUV pulse found in two-dimensional simulation is also longer, it is still within 1 fs.

Figure 7 shows comparison of the APs produced in the uniform and non-uniform plasma. In non-uniform plasma, the AP has a full duration about 900*as*, which is still shorter than that found in uniform plasma. Besides, its peak amplitude reaches about 10, corresponding to the intensity of 1.7×10^{20} W/cm^2, which is three times larger than that found in one-dimensional simulation. The transverse effects of a finite spot size are associated with the wakefield structure in the two-dimensional geometry, which is similar to that found previously (Liu *et al.*, 2012). When a high-intensity laser pulse enters the plasma from the vacuum, it pushes the local electrons out of their paths both longitudinally and transversely, producing an open cavity bounded by an electron-rich sheath. For such an ultra-intense laser presented here with a large spot size, the resulting electron density structure resembles a bow cavity in the first wake rather than a spherical shape behind the laser pulse. As the laser pulse passes through the up-ramp and enters the uniform density region, a thin electron sheet emerges at the rear of the cavity, which is trapped and longitudinally compressed. Meanwhile, a strong transverse radial electric field is produced inside the cavity, which tends to focus the trapped electron sheet transversely. In the present simulation, the electron sheet finally focused to a transverse size around 4 μm near the laser axis, resulting in a much higher electron peak density than the one-dimensional case. As a result, the produced current density is higher and its width is larger than that in the one-dimensional case. This explains why the AP has a higher amplitude and a longer duration in the two-dimensional simulation.

4. SUMMARY

We have proposed a scheme to generate ultra-intense APs from laser wakefield excitation in non-uniform under-dense plasma. A high electron density spike generated in the laser wakefield and the residual transverse electron momentum left behind the laser pulse can lead to the formation of a transverse current sheet, which emits APs. It is found that there is a positive feedback process in the AP formation. As soon as the density spike and the small residual transverse electron momentum at the density spike appear, a small amplitude AP emerges. Then the newly produced AP field immediately

https://doi.org/10.1017/S0263034613000220 Published online by Cambridge University Press

feeds back in a way to enhance the transverse electron momentum and the transverse current. Consequently, the APs are further enhanced. This positive loop continues until the interaction process terminates when the density spike behind the laser pulse disappears due to the pump laser depletion.

It is shown that an up-ramp density profile in front of a uniform plasma slab can be used to generate APs with much higher peak intensity and shorter pulse duration. If the driving laser is circularly polarized, the produced AP is also circularly-polarized. Simulation reveals that such AP emission can be observed in a wide laser and plasma parameter regime. Our scheme may pave the way towards giant single attosecond pulse with both simplicity and robustness.

ACKNOWLEDGEMENTS

The authors would like to acknowledge the OSIRIS Consortium, consisting of UCLA and IST (Lisbon, Portugal) for providing access to the OSIRIS 2.0 framework. This work is supported by the National Science Foundation of China (Grant No. 11121504 and 11075105). The computational resources utilized in this research were provided partially by Shanghai Supercomputer Center.

REFERENCES

Baeva, T., Gordienko, S. & Pukhov, A. (2007). Relativistic plasma control for single attosecond pulse generation: Theory, simulations, and structure of the pulse. *Laser Part. Beams* **25**, 339–346.

Bulanov, S., Naumova, N., Pegoraro, F. & Sakai, J. (1998). Particle injection into the wave acceleration phase due to nonlinear wake wave breaking. *Phys. Rev. E* **58**, R5257.

Bulanov, S.V., Esirkepov, T. & Tajima, T. (2003). Light intensification towards the schwinger limit. *Phys. Rev. Lett*. **91**, 085001.

Chen, M., Sheng, Z.M., Zheng, J., Yanyun, M.A. & Zhang, J. (2008). Development and application of multi–dimensional particle-in-cell codes for investigation of laser plasma interactions. *Chin. J. Comput. Phys*. **25**, 43.

Corkum, P.B. & Krausz, F. (2007). Attosecond science. *Nat. Phys*. **3**, 381.

Decker, C.D., Mori, W.B., Tzeng, K.C. & Katsouleas, T. (1996). Evolution of ultra-intense, short-pulse lasers in underdense plasmas. *Phys. Plasmas* **3**, 2047.

Dromey, B., Rykovanov, S.G., Adams, D., Horlein, R., Nomura, Y., Carroll, D.C., Foster, P.S., Kar, S., Markey, K., McKenna, P., Neely, D., Geissler, M., Tsakiris, G.D. & Zepf, M. (2009). Tunable enhancement of high harmonic emission from laser solid interactions. *Phys. Rev. Lett*. **102**, 225002.

Fonseca, R.A., Silva, L.O., Tsung, F.S., Decyk, V.K., Lu, W., Ren, C., Mori, W.B., Deng, S., Lee, S., Katsouleas, T. & Adam, J.C. (2002). Osiris: A three-dimensional, fully relativistic particle in cell code for modeling plasma based accelerators. In *Lecture notes in computer science* Sloot, P., Tan, C.J.K., Dongarra, J.J. and Hoekstra, A.G., Eds.). New York: Springer, Vol. 2331, pp. 342–351.

Hergott, J.F., Kovacev, M., Merdji, H., Hubert, C., Mairesse, Y., Jean, E., Breger, P., Agostini, P., Carre, B. & Salieres, P. (2002). Extreme-ultraviolet high-order harmonic pulses in the microjoule range. *Phys. Rev. A* **66**, 021801.

Kando, M., Fukuda, Y., Pirozhkov, A.S., Ma, J., Daito, I., Chen, L.M., Esirkepov, T.Z., Ogura, K., Homma, T., Hayashi, Y., Kotaki, H., Sagisaka, A., Mori, M., Koga, J.K., Daido, H., Bulanov, S.V., Kimura, T., Kato, Y. & Tajima, T. (2007). Demonstration of laser-frequency upshift by electron-density modulations in a plasma wakefield. *Phys. Rev. Lett*. **99**, 135001.

Li, F.Y., Sheng, Z.M., Liu, Y., Meyer-Ter-Vehn, J., Mori, W.B., Lu, W. & Zhang, J. (2013). Dense attosecond electron sheets from laser wakefields using an up-ramp density transition. *Phys. Rev. Lett*. **110**, 135002.

Liu, Y., Sheng, Z.M., Zheng, J., Li, F.Y., Xu, X.L., Lu, W., Mori, W.B., Liu, C.S. & Zhang, J. (2012). Ultrafast xuv emission from laser wakefields in underdense plasma. *New J. Phys*. **14**, 083031.

Meyer-ter-Vehn, J. & Wu, H.C. (2009). Coherent Thomson backscattering from laser-driven relativistic ultra-thin electron layers. *Eur. Phys. J. D*. **55**, 433–441.

Midorikawa, K. (2011). High-order harmonic generation and attosecond science. *Jpn. J. Appl. Phys*. **50**, 090001.

Mourou, G.A., Labaune, C.L., Dunne, M., Naumova, N. & Tikhonchuk, V.T. (2007). Relativistic laser-matter interaction: From attosecond pulse generation to fast ignition. *Plasma Phys. Contr. Fusion* **49**, B667–B675.

Nabekawa, Y., Shimizu, T., Furukawa, Y., Takahashi, E.J. & Midorikawa, K. (2009). Interferometry of attosecond pulse trains in the extreme ultraviolet wavelength region. *Phys. Rev. Lett*. **102**, 213904.

Naumova, N.M., Nees, J.A., Sokolov, I.V., Hou, B. & Mourou, G.A. (2004). Relativistic generation of isolated attosecond pulses in a lambda(3) focal volume. *Phys. Rev. Lett*. **92**, 063902.

Quere, F., Thaury, C., Monot, P., Dobosz, S., Martin, P., Geindre, J.P. & Audebert, P. (2006). Coherent wake emission of high-order harmonics from overdense plasmas. *Phys. Rev. Lett*. **96**, 125004.

Roso, L., Plaja, L., Rzazewski, K. & von der Linde, D. (2000). Beyond the moving mirror model: Attosecond pulses from a relativistically moving plasma. *Laser Part. Beams* **18**, 467–475.

Salieres, P., Huillier, A.L. & Lewenstein, M. (1995). Coherence control of high-order harmonics. *Phys. Rev. Lett*. **74**, 3776.

Sheng, Z.M., Sentoku, Y., Mima, K., Zhang, J., Yu, W. & Meyer-ter-Vehn, J. (2000). Angular distributions of fast electrons, ions, and bremsstrahlung X/gamma-rays in intense laser interaction with solid targets. *Phys. Rev. Lett*. **85**, 5340.

Takahashi, E.J., Nabekawa, Y. & Midorikawa, K. (2004). Low-divergence coherent soft x-ray source at 13 nm by high-order harmonics. *Appl. Phys. Lett*. **84**, 4.

Tsakiris, G.D., Eidmann, K., Meyer-ter-Vehn, J. & Krausz, F. (2006). Route to intense single attosecond pulses. *New J. Phys*. **8**, 19.

Von der Linde, D., Sokolowski-Tinten, K., Blome, C., Dietrich, C., Zhou, P., Tarasevitch, A., Cavalleri, A., Siders, C.W., Barty, C.P.J., Squier, J., Wilson, K.R., Uschmann, I. & Forster, E. (2001). Generation and application of ultrashort x-ray pulses. *Laser Part. Beams* **19**, 15–22.

Wang, W.M., Sheng, Z.M., Norreys, P.A. Sherlock, M., Trines, R., Robinson, A.P.L., Li, Y.T., Hao, B., Zhang, J. (2010). Electron energy deposition to the fusion target core for fast ignition. *J. Phys.: Conf. Ser*. **244**, 022070.

Wu, H.C., Meyer-ter-Vehn, J., Fernandez, J. & Hegelich, B.M. (2010). Uniform laser-driven relativistic electron layer for coherent thomson scattering. *Phys. Rev. Lett*. **104**, 234801.

Zheng, J., Sheng, Z.M., Zhang, J., Chen, M. & Ma, Y.Y. (2006). Effects of laser intensities and target shapes on attosecond pulse generation from irradiated solid surfaces. *Chin. Phys. Lett*. **23**, 377–380.